

Article

Bismuth Polycations Revisited: Alternative Synthesis and Electronic Structure of Bi_6Br_7 , and Bonding in Main-Group Polyatomic Ions from a Direct Space Perspective

Ekaterina A. Stroganova¹, Sergey I. Troyanov¹, Igor V. Morozov¹ and Alexey N. Kuznetsov^{1,2,*} 

¹ Department of Chemistry, Lomonosov Moscow State University, Leninskie Gory 1-3, 119991 Moscow, Russia; stroganova@inorg.chem.msu.ru (E.A.S.); stroyano@thermo.chem.msu.ru (S.I.T.); morozov@inorg.chem.msu.ru (I.V.M.)

² Kurnakov Institute of General and Inorganic Chemistry of RAS, Leninskii pr. 31, 119991 Moscow, Russia

* Correspondence: alexei@inorg.chem.msu.ru; Tel.: +7-495-939-5502

Received: 17 September 2020; Accepted: 15 October 2020; Published: 16 October 2020



Abstract: A bismuth subbromide, Bi_6Br_7 , was synthesized in the form of single crystals using the reaction between Bi and Hg_2Br_2 in a gradient furnace. Its crystal structure was reinvestigated by low-temperature single-crystal X-ray diffraction ($Pn\bar{m}$, $a = 15.4996(6)$ Å, $b = 23.6435(7)$ Å, $c = 9.0231(2)$ Å, $Z = 8$, $R_1 = 0.041$, $wR_{\text{all}} = 0.087$). Based on the diffraction data, the structure description was revised as containing Bi_9^{5+} cluster polycations and $^{1\infty}[\text{Bi}_3\text{Br}_{14}^{5-}]$ ladder-like anions. DFT calculations of band structure showed the compound to be a narrow-gap semiconductor with a band gap of ca. 1.3 eV, with the nature of the compound as ionic salt confirmed by charge density analysis. Direct-space bonding analysis based on the ELF topology and QTAIM partitioning, performed for all known homoatomic bismuth polycations, as well as isoelectronic main-group metal ions, shows patterns of localized pairwise and three-center bonding forming the frameworks of the clusters. In addition to obtaining new data, the use of highly augmented basis sets allowed us to revise and amend several previously made conclusions regarding bonding in such species.

Keywords: metal-metal bonds; main-group clusters; bismuth polycations; subvalent halides; crystal structure; DFT calculations; band structure; ELF

1. Introduction

From a chemical point of view, bismuth is a pretty remarkable element, which in a textbook sense, has only a couple of stable oxidation states. However, in the real world, bismuth has incredibly rich subvalent chemistry, for which it was coined “The Wonder Metal” by J.D. Corbett [1], one of the pioneers of bismuth cluster studies. And that was before the true diversity of bismuth subvalent compounds was known! Among particularly interesting objects in the field are bismuth cluster polycations, i.e., electron-deficient polyatomic clusters of varying geometry. The first solid compound containing bismuth cluster polycation was bismuth “monochloride” Bi_6Cl_7 [2], discovered in the early 60s, and the cation was Bi_9^{5+} . In the next six decades, other binary and ternary compounds featuring this cation followed [3–13]. A number of other species were also discovered, such as ‘classical’ Bi_5^{3+} [14–19] and Bi_8^{2+} [13,14,20–24], and more recent additions Bi_5^{2+} [25,26], Bi_6^{2+} [26,27], and Bi_{10}^{4+} , although the latter has not been obtained as a true homoatomic unity and was mostly centered by palladium or platinum, or on rare occasion even by gold [28–31] (we leave its capped forms outside the scope of this paper as their homoatomic nature is questionable, as well as other heteroatomic bismuth clusters). The compounds that contain these polycations are essentially complex

salts, with counterions for bismuth clusters being metal halide anions. They are typically synthesized either from melts or non-aqueous solutions. A comprehensive review of synthetic approaches to polycations of group 15–16 elements is given in [32], with additional information on the use of ionic liquids provided in [33]. From a topological point of view, these bismuth clusters are fairly unique, however, not completely without relatives. Bismuth's lighter group 15 neighbor, antimony, features far less abundant homopolyatomic cation chemistry, although Sb_5^{3+} [16] and Sb_8^{2+} [17,34] have been reported, both having matching polyhedral bismuth counterparts. And then there are also naked clusters of group 14 elements, Zintl ions E_5^{2-} and E_9^{4-} ($\text{E} = \text{Si}, \text{Ge}, \text{Sn}, \text{Pb}$) [35], appearing in various intermetallic and coordination compounds, which are isoelectronic and (more or less) isostructural to Bi_5^{3+} and Bi_9^{5+} , although to maintain the same electron count they obviously need to be anions.

The compounds that feature bismuth cluster polycations turned out to be rather difficult to work with, due to them often being air- and moisture-sensitive, and particularly complex objects for the X-ray crystallography, for both technical and fundamental reasons (e.g., a tendency to show pseudo-symmetry or form disordered arrangements) [22,24]. As a consequence, some of the reported structures, particularly those from earlier times, were plagued by errors. The quality of structure determination was much improved in more recent times. Some of the older structures, like Bi_6Cl_7 and $\text{Bi}_8(\text{AlCl}_4)_2$ [36], were re-determined with improved quality, which in the case of Bi_6Cl_7 , led to a slight reinterpretation of its anionic arrangement. More recently, in 2013, these two structures were reinvestigated again, based on the XRD data obtained from crystals synthesized in ionic liquids [37]. Bi_6Br_7 was also recently synthesized using the reaction of bismuth with its tribromide in $[\text{BMIm}]\text{Cl} \cdot 2\text{AlCl}_3$ [37]. Its crystal structure was reinvestigated by low-temperature single-crystal XRD, however, the authors provided no description of structural details.

In our studies, initially focused on optimizing crystal growth technique for another bismuth subbromide, Bi_4Br_4 , we have come up with an alternative way of producing crystals of Bi_6Br_7 . Having obtained good quality single crystals, we investigated them by means of XRD, primarily to see if there were differences with what was already reported on the compound. And since the structure description still stood as it was given in 1978, we decided to update it based on our data. Improved structure description and atom localization gave us an opportunity to reliably study the band structure of the compound and the topology and bonding in polycations.

To put electronic structure and bonding information in proper context, we also reinvestigated bonding in bismuth polycations and related isoelectronic homoatomic main-group clusters within the concept of R. Bader's Quantum theory of atoms in molecules (QTAIM) [38] via topological analysis of the electron localization function (ELF) [39–41]. Almost exactly twenty years ago, bonding analysis, based on a combination of natural bond orbital analysis and ELF topology for bismuth polycations that were known at the time, was reported [42], which was the first comprehensive study of this type. However, with bonding not being the main focus of the study, and with ELF being in its relatively early days of practical use, some of the conclusions made within that paper were not entirely solid. Since then, with the rapid progress of the density functional theory (DFT) applications in chemistry and growing number of bonding analysis tools, along with the discovery of new clusters and emergence of more in-depth approaches to the analysis of bonding indicators, the need to revisit and update that material has been long overdue (although selected cations have received better treatment in more recent publications [10,28–30]). With this research, we offer a sufficiently expanded and amended picture of homoatomic bonding in bismuth cluster polycations and their isoelectronic analogues of group 14 and 15 from the point of direct-space analysis.

2. Materials and Methods

2.1. Synthesis and Primary Characterization

Bismuth metal (powder, 99.98%) and Hg_2Br_2 (99.8%) were used as starting materials for the synthesis. A batch of 1.15 g of Bi and 2.33 g of Hg_2Br_2 was placed into a silica tube (210 mm long,

16 mm in diameter), flame-sealed under vacuum (ca. 10^{-2} Torr), and placed into a horizontal gradient furnace, with the temperatures at the opposite ends of the tube being 230 and 265 °C. Chemicals were placed at the hotter end. The experiment was kept running for 6 days, after which it was cooled down to room temperature. Visual inspection of the tube showed two kinds of crystals formed, elongated prismatic (or thick needle-like) ones near the colder end of the tube, and thin needles almost above the starting materials. Both types of crystals were black with a hint of metallic luster; also visible in the tube was liquid mercury.

Energy dispersive X-Ray spectroscopy (EDS) using Jeol/Nikon Neoscope 6100 ($U_{acc} = 20$ kV, internal calibration, 3–5 points per crystal) showed both the types of crystals to be binary bismuth bromides, with the first type having Bi:Br ratio of 1, and the second of 0.88, which allowed us to identify the compounds as Bi_4Br_4 and Bi_6Br_7 , respectively. The latter appeared as well-shaped rectangular crystals up to 1 mm long with a thickness of ca. 0.2–0.3 mm. This appears as a bit of a surprise, since the method involving chemical transport with $HgBr_2$ [4] or Hg_2Br_2 [43] was supposed to produce Bi_4Br_4 , while the other subbromide was described as forming from Bi- $BiBr_3$ melts [4]. However, the location of Bi_6Br_7 crystals at the top side of a tube indicated that the gas phase reaction was involved in crystal growth. The binary Bi-Br system is rather unique among the Bi-X systems ($X = Cl, Br, I$), since it features both salt-like polycationic subhalides like Bi_6Br_7 and bismuth subhalides with extended bismuth fragments of the Bi_4Br_4 family, while for $X = Cl$ only polycation-containing phases exist, and for $X = I$ only subhalides with extended structures are found. And the way of separating them was to use different synthetic conditions. Obviously, to stabilize bismuth polycations, suitable anions must be present in the system, which makes synthetic approaches involving $BiBr_3$ melts or $BiBr_3$ -containing solutions highly favorable. In our case, we do not introduce extra $BiBr_3$ in the system, so the anionic part in our case must be formed in the process of redox reactions involving Bi and Hg_2Br_2 .

2.2. X-ray Crystallography

X-ray diffraction data for a suitable single crystal of Bi_6Br_7 was recorded at 100 K using automated Stoe IPDS diffractometer (graphite monochromator, MoK_{α} -radiation, $\lambda = 0.71073$ Å) equipped with Imaging Plate detector. The structure was solved by direct methods and refined against F_o^2 using SHELX-2018 package [44]. Data collection and structure refinement details, as well as atomic coordinates and atomic displacement parameters, are given in Tables S1 and S2, respectively, in the Supplementary Materials. Select interatomic distances are given in Table 1. A summary of crystallographic data for the single-crystal experiment is available from CCDC (ref. number 2032218).

Table 1. Selected interatomic distances for Bi_6Br_7 .

Atoms	Distance, Å	Atoms	Distance, Å	Atoms	Distance, Å
Bi(1)-Bi(1)	3.1847(17)	Bi(3)-Bi(4)	3.1008(12)	Bi(8)-Br(8)	2.938(3)
Bi(1)-Bi(3)	3.1229(10)	Bi(7)-Br(1)	3.024(2)	Bi(8)-Br(11)	2.739(3)
Bi(1)-Bi(5)	3.1244(11)	Bi(7)-Br(3)	2.913(2)	Bi(9)-Br(2)	2.736(2)
Bi(1)-Bi(6)	3.2245(12)	Bi(7)-Br(5)	3.037(3)	Bi(9)-Br(4)	3.017(2)
Bi(2)-Bi(2)	3.3017(17)	Bi(7)-Br(9)	2.775(3)	Bi(9)-Br(6)	2.781(3)
Bi(2)-Bi(3)	3.1443(11)	Bi(7)-Br(10)	3.112(3)	Bi(9)-Br(10)	3.013(3)
Bi(2)-Bi(4)	3.1646(13)	Bi(8)-Br(1)	2.872(2)		
Bi(2)-Bi(5)	3.0855(12)	Bi(8)-Br(3)	3.148(2)		
Bi(3)-Bi(6)	3.0821(11)	Bi(8)-Br(7)	2.787(3)		

2.3. Computational Details

Band structure calculations on crystalline Bi_6Br_7 were performed on the density-functional theory (DFT) level utilizing the Projector Augmented Wave method (PAW) as implemented in the pseudopotential Vienna Ab initio Simulation Package (VASP) code [45,46]. For the modeling, experimentally determined structure was transformed into the $P1$ space group. The PBE exchange-correlation functional [47] of the GGA-type was used in the calculations. Spin-orbit coupling

was accounted for in the calculations. The energy cut-off was set at 500 eV with a $12 \times 6 \times 12$ Monkhorst-Pack [48] k -point mesh used for Brillouin zone sampling. Atomic charges were analyzed according to Bader's QTAIM approach [38].

Isolated cluster calculations were performed on the DFT level using hybrid B3LYP [49,50] exchange-correlation functional as implemented in the Orca 4.2.1 package [51,52]. For the polycations, a combination of def2-QZVPPD [53] basis sets and relativistic effective core potentials (ECP) was used: 60-electron core ECP60MDF [54] for Bi and Pt, 28-electron core ECP28MDF [54] for Sb and Pd. For the geometry optimizations of polyanions, ma-def2-TZVPP [55] basis sets were used, all-electron for Ge, and in combination with ECP28MDF for Sn and ECP60MDF for Pb. For energy calculations for optimized structures, def2-QZVPPD basis sets with respective ECP's were used. Constrained optimization retaining point symmetry group was performed.

The electron localization function (ELF) was calculated and analyzed using the Multiwfn 3.7 package [56]. Structure visualization was done using the VESTA package [57]. Band structures near the Fermi level were plotted using the wxDragon package [58].

3. Results and Discussion

3.1. Crystal Structure of Bi_6Br_7 and the Geometry of Bi_9^{5+}

The crystal structure of Bi_6Br_7 is shown in Figure 1, and isolated bismuth polycations in Figure 2.

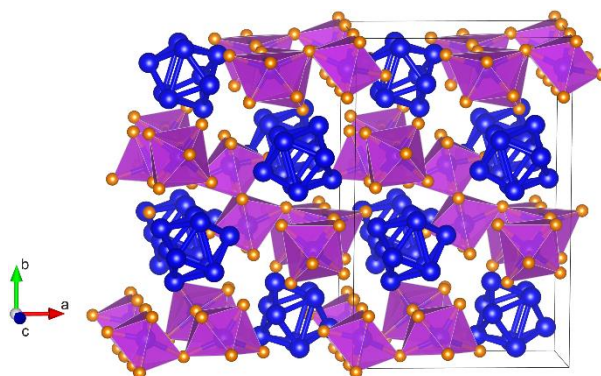


Figure 1. Polyhedral representation of the crystal structure of Bi_6Br_7 . Bismuth atoms are shown in blue, bromine in orange. Black lines depict the unit cell.

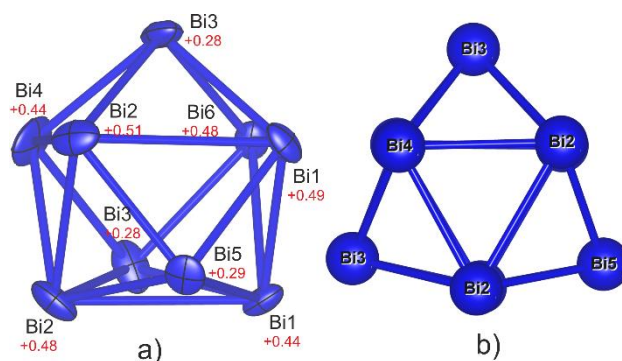


Figure 2. The geometry of Bi_9^{5+} in Bi_6Br_7 : (a) side view with thermal ellipsoids (99% probability) and atomic charges (in red); (b) a view down the three-fold axis.

The experiment at low temperature, with a relatively small but well-shaped and well-reflecting single crystal, produced the results that generally agree with the data published in [37], which significantly improves atom localization and atomic coordinates as compared to [4]. This leads to interatomic distances precision improved by ca. half an order of magnitude. In [4], the average esd

in Bi-Bi bond length is ca. 0.007 Å, while in our refinement, it is ca. 0.0013 Å. Similarly, the average esd in Bi-Br bond length was improved from ca. 0.015 [4] to ca. 0.0026 Å. The results from [37] are very similar to ours. Apparently, different synthetic approaches did not lead to variations in the structure.

The authors of [37] decided not to make direct comparisons to the structure from 1978, citing large temperature differences of analysis, making such comparisons not applicable. We do not believe that in this case, major effects take place, like phase transition, which separate the data obtained at 100 and 298 K. In fact, the comparison of our data with [4] and [37] confirms this is not the case, and the structure is essentially the same. The results of side-by-side comparisons of the crystallographic data from this work, [4], and [37], performed with the help of COMPSTRU routine [59], are given in Supplementary Materials (Tables S3–S11). Therefore we think that the discussion of the structure after redetermination at low temperature is valuable and relevant to room temperature. Such discussion is particularly important since it affects further studies of the electronic structure of the compound. The general description of the structure remains similar to that obtained at room temperature in 1978 [4], especially in the cationic part. Bi_9^{5+} polycations in the structure (see Figure 2) are close to the D_{3h} symmetry (trigonal tricapped prism) and feature Bi-Bi distances in the 3.082–3.302 Å range, while in [4] they are characterized as being inbetween D_{3h} and C_{4v} (monocapped square antiprism) symmetries, but better described by D_{3h} , with the interatomic distances falling into the 3.087–3.320 Å range. Our data show, based on the thermal ellipsoid analysis, that the cations are not prone to the significant orientational disorder and rather well-localized.

Following the logic of the authors of [36], who changed the description of the anionic part of Bi_6Cl_7 from isolated anions to a polymer-like framework, and based on our own analysis of crystallographic data, the description of the anionic part of the structure of Bi_6Br_7 also needs to be revised as compared to that provided in [4], where it was described as consisting of BiBr_5^{2-} (Bi-Br = 2.798–3.148 Å) and $\text{Bi}_2\text{Br}_8^{2-}$ (Bi-Br = 2.742–3.066 Å) anions. In fact, there are chains of polyhedra along the c axis linked by two bromine atoms each (Br1 and Br3), Br1 at the distances of ca. 2.87 and 3.02 Å from Bi8 and Bi7, respectively, and Br3 at 3.15 and 2.91 Å from the respective bismuth atoms (see Figure 3a). We prefer to describe these polyhedra as edge-sharing, but even if one chooses to discard 3.15 Å as the non-bonding distance (although in [4] it is a part of the BiBr_5^{2-} unit), the polyhedra would still be linked via the Br1 vertices at 2.87/3.02 Å. And $\text{Bi}_2\text{Br}_8^{2-}$ are linked to the polymer chains by Br10 atoms at ca. 3.11 Å, while the longest intra-anion distance is ca. 3.02 Å, i.e., less than 3% shorter. Based on these considerations, we suggest the description where bismuth and bromine form polymer-like bromobismuthate anion ${}^1_\infty[\text{Bi}_3\text{Br}_{14}^{5-}]$ (Bi-Br = 2.775–3.148 Å) that consists of edge-sharing bismuth-centered bromine polyhedra, forming one-dimensional chains along the c axis, linked via vertices by dimeric edge-sharing BiBr_6 octahedral units (see Figure 3). Thus, ${}^1_\infty[\text{Bi}_3\text{Br}_{14}^{5-}]$ forms a ladder-like framework with side rails formed by pentagonal bipyramids and rungs by edge-sharing octahedra (see Figure 3a). The voids left by missing rungs are filled with bismuth polycations, forming two Bi-Br contacts with a length of 3.266 Å. This picture is similar to the one provided in [36] for Bi_6Cl_7 , which is only logical since these two compounds are isotopic. Based on the comparison of our data with that published in [37] for Bi_6Cl_7 and Bi_6Br_7 (see Supplementary Materials, Tables S12–S14), we believe that this conclusion is consistent with the data.

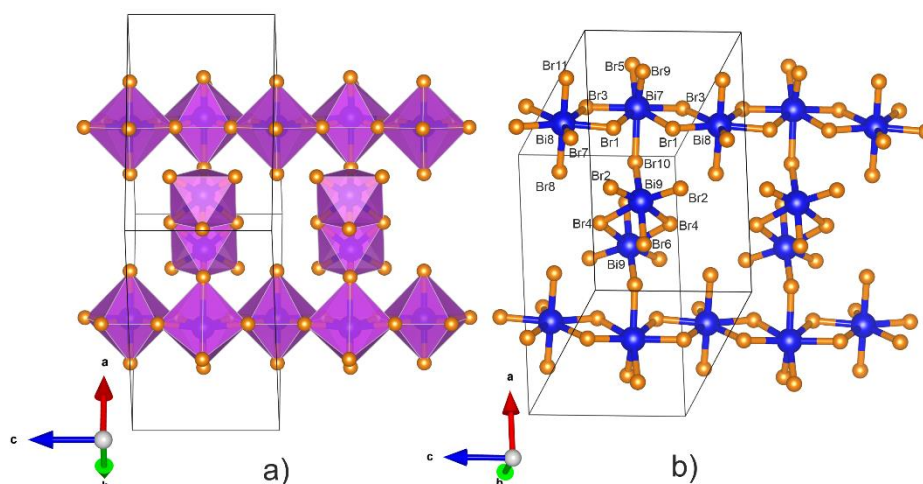


Figure 3. Anionic part of the Bi_6Br_7 structure with $^{1\infty}[\text{Bi}_3\text{Br}_{14}^{5-}]$ strands: (a) polyhedral representation; (b) ball-and-stick view.

3.2. Electronic Structure of Bi_6Br_7

Band structure of Bi_6Br_7 was evaluated based on the DFT calculations. Figure 4 shows the calculated total (TDOS) and projected (PDOS) density of states (DOS) plot near the Fermi level. According to the calculations, Bi_6Br_7 is a narrow-gap semiconductor with the band gap value of ca. 1.3 eV. The top of the valence band features major contributions from Bi 6p-states of Bi_9^{5+} and bromine 4p-states, and a relatively minor contribution from Bi 6p-states from polymeric bromobismuthate anions. Polycationic bismuth 6s pairs are located over 9 eV below the Fermi level and are very well localized, thus confirming their chemical inertness. The bottom of the conduction band is contributed equally by p-states of Bi and Br from the anions, but the major contribution is from 6p-states of Bi in Bi_9^{5+} . All these states are located in the same energy range, which means that electronic transport can be conducted between bismuth and bromine states in the anionic framework, which explains the predicted narrow-gap semiconductor behavior of the compound. However, based on the contributions from Bi_9^{5+} 6p-states to the conduction and valence bands, we cannot completely rule out that polycations may participate in the electric conductivity, rather than the latter being facilitated through the anionic framework only. This appears to be surprising for the compound built like an ionic salt, however, looking at the Bi-Br contacts, we observe that the longest inter-anionic distances of 3.112 Å (or 3.149 Å, depending on vertex- or edge-sharing model) are just ca. 0.15 Å (or ca. 0.12 Å) shorter than the shortest distance from Bi_9^{5+} to Br ($\text{Bi}_2\text{-Br}_8 = 3.266$ Å), which might explain how bismuth clusters may theoretically participate in the electronic transfer.

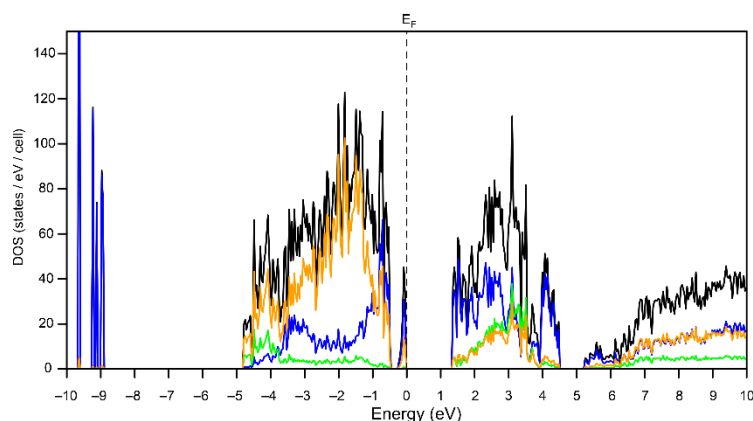


Figure 4. Total (black line) and projected (Bi in Bi_9^{5+} —blue line, Bi in $[\text{Bi}_3\text{Br}_{14}^{5-}]$ —green line, Br—orange line) DOS near the Fermi level for Bi_6Br_7 .

Atomic charges calculated according to the QTAIM approach are: $+0.28 \div +0.51$ (Bi in Bi_9^{5+} , for more detail see Figure 2), $+1.43 \div +1.45$ (Bi in $[\text{Bi}_3\text{Br}_{14}^{5-}]$), $-0.59 \div -0.61$ (Br), and the average calculated charge for Bi_9 is ca. $+3.7$, and its counterion ca. -3.7 , instead of $+5$ and -5 , respectively. Yet, these are still very high calculated charges, considering that Bi in the polyanion, which is formally $+3$, has a calculated charge of less than $+1.5$. Therefore, we may conclude that the description of this compound as an ionic salt still holds well, and there are obviously strong ionic interactions between the counterparts in the structure.

3.3. Bonding in Bismuth Polycations and Isoelectronic Main-Group Metal Clusters: 3D-Aromaticity vs. Localized Bonding

Bonding was investigated by analyzing ELF topology for isolated clusters. ELF has three types of attractors, namely atomic shells, lone pairs, and localized chemical bonds, and it is the latter type that is of special interest to us, since it shows us bonding interactions in the clusters. By integrating electron density over the bonding ELF basins, we can quantify the number of electrons participating in bonding for each particular attractor. Geometries and ELF isosurfaces for bismuth polycations and isoelectronic main-group metal clusters are depicted in Figure 5, and symmetry and bond basin characteristics in Table 2.

Before moving to the analysis of specific clusters, general observation must be made on the ELF basis dependence. This function is generally considered very robust and fairly insensitive to a computational method. This may well be true as far as the level of theory is concerned, however, ELF might be sensitive towards basis sets used, as discussed in [60]. While evaluating computational conditions for the ELF calculations for post-transition elements, we have found out that a basis set well augmented with polarization and diffuse functions is essential to observe all the ELF features. For instance, the use of reliable energy-optimized LANL2DZ Los Alamos valence double-zeta basis with Hay-Wadt ECP [61] or its triple-zeta LANL2TZ version leads to almost no non-atomic centered ELF attractors visible while scanning the localization parameter. The use of more advanced Stuttgart/Dresden family ECPs [62] does not change the picture, as long as they are paired with DZ or TZ quality basis sets with minimum diffuse or polarization functions. We did not specifically study the effect of small core (SC) vs. large core (LC) ECPs on ELF, yet a limited number of tests indicates that 60-electron core ECPs produce better results for Bi and Pb than 78-electron core ones.

3.3.1. Five-vertex Polyhedra

Five vertex polyhedra are represented by isoelectronic Bi_5^{3+} , Sb_5^{3+} , Ge_5^{2-} , Sn_5^{2-} , Pb_5^{2-} in the shape of trigonal bipyramid, and a single Bi_5^+ as a square pyramid. The ELF topology of the latter shows four non-atomic attractors, which are localization domains corresponding to the Bi-Bi disynaptic bond basins in the base of the pyramid (Ω_1), appearing at higher localization parameter (η) values, and another four domains (disynaptic Ω_2) corresponding to the bonds between the base and the apical atom at lower η values (see Figure 5). The integration of electron density gives us basin populations of ca. $1.8 e$ for Ω_1 and ca. $0.9 e$ for Ω_2 . Thus, this cluster has four almost $2c,2e$ -bonds in its base, and the apical atom is bonded to the base via four $1e$ -bonds. Quantitative part aside (as there was no basin population analysis done), this is very close to what the authors of [42] observed using ELF. However, the authors were laboring upon the assumption that $\eta = 0.5$ means “perfectly delocalized electrons”, and thus observing Bi-Bi bonds to apical Bi at $\eta = 0.53$, they called them “almost fully delocalized”. This rather common misinterpretation of ELF has been corrected since then [63]. All the ELF range from 0 to 1 is eligible for analysis, and, in fact, some bonds, particularly transition metal-based, only appear below $\eta = 0.5$, which does not make them perfectly delocalized. By its nature, ELF is only capable of displaying regions of electron localization so that truly delocalized electrons, such as conduction electrons, cannot be seen in ELF. Another possible source of misinterpretation of bonding in these objects is the mix-up between delocalized and multi-center bonds. ELF is perfectly capable of displaying the latter, but has not been intended to show the former. Therefore, multi-center bonds

observed in the ELF topology can only be called ‘delocalized’ in the sense that they are not localized between pairs of atoms or in terms of a small number of electrons localized within bond basins. The results of the NBO analysis for Bi_5^+ were better and worse at the same time. Better because they correctly predicted localized bonding between the base and the apex, and worse because they showed only three bonds and broke the symmetry of the cluster. Now we can revise the description of the bonding in Bi_5^+ and show the essentially localized nature of bonding in it.

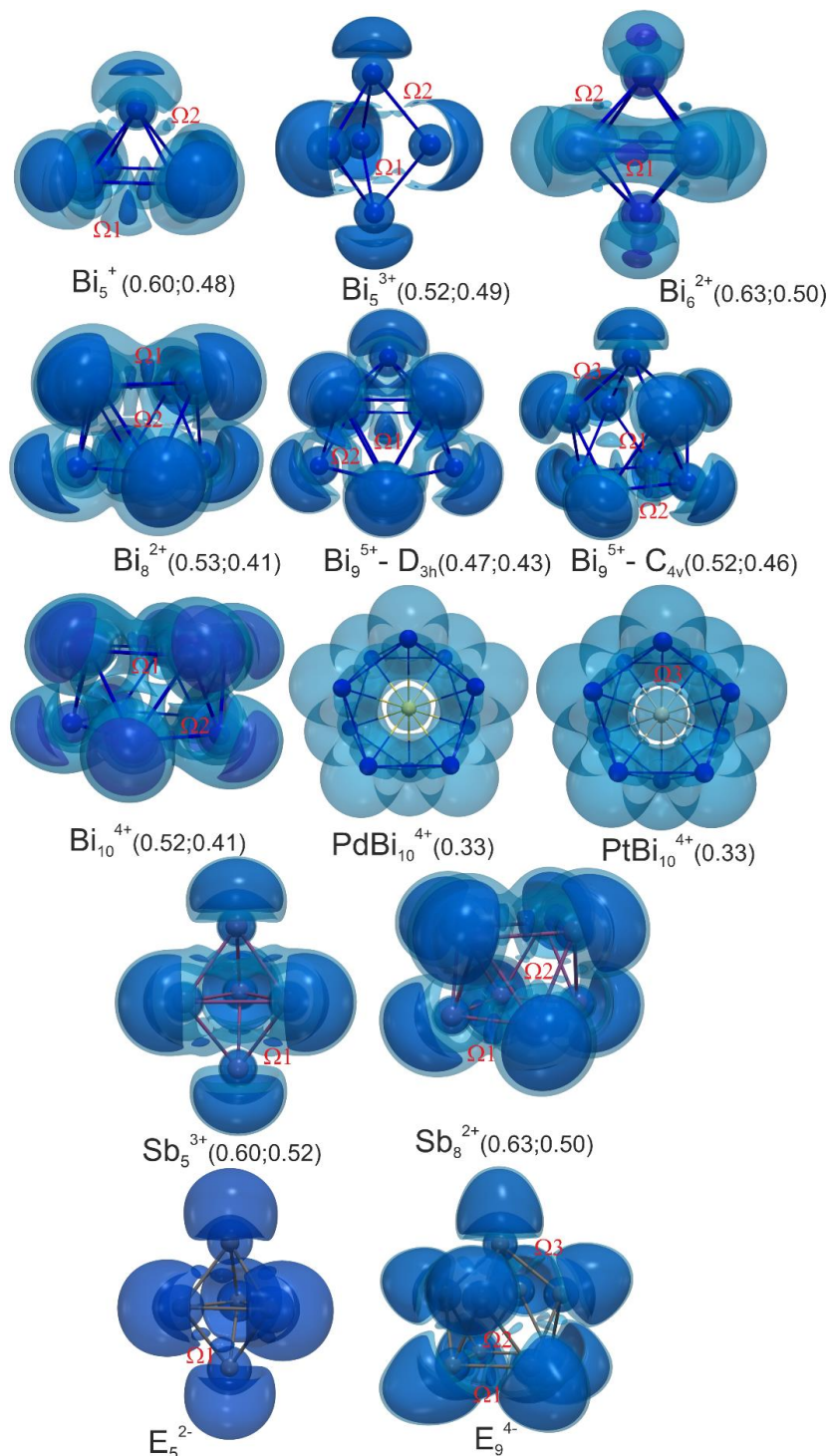


Figure 5. Geometries and ELF isosurfaces for bismuth polycations and isoelectronic main-group metal clusters. The figures in parentheses denote localization parameter η_1 (deep blue) and η_2 (light blue), separated by a semicolon, at which isosurfaces are drawn. For the explanation of Ω_1 – Ω_3 see the text.

Table 2. Symmetries of optimized structures and bond basin populations for main-group clusters.

Polyion	Symmetry	Basin Population, <i>e</i>		
		$\Omega 1$	$\Omega 2$	$\Omega 3$
Bi ₅ ⁺	C _{4v}	1.81	0.84	-
Bi ₅ ³⁺	D _{3h}	0.72	0.70	-
Bi ₆ ²⁺	D _{4h}	1.45	0.95	-
Bi ₈ ²⁺	D _{4d}	1.61	0.21	-
Bi ₉ ⁵⁺	D _{3h}	1.36	1.17	-
Bi ₉ ⁵⁺	C _{4v}	1.36	1.57	1.02
Bi ₉ ⁵⁺ (Bi ₆ Br ₇)	C _S	1.19	0.89/0.83	
Bi ₁₀ ⁴⁺	D _{5d}	1.83	1.03	-
PdBi ₁₀ ⁴⁺	D _{5d}	0.85	0.58	0.21
PtBi ₁₀ ⁴⁺	D _{5d}	0.83	0.58	0.33
Sb ₅ ³⁺	D _{3h}	1.7	-	-
Sb ₈ ²⁺	D _{4d}	1.52	0.51	-
Ge ₅ ²⁻	D _{3h}	1.33	-	-
Ge ₉ ⁴⁻	C _{4v}	1.06	0.99	0.96
Sn ₅ ²⁻	D _{3h}	1.35	-	-
Sn ₉ ⁴⁻	C _{4v}	0.95	0.94	0.92
Pb ₅ ²⁻	D _{3h}	0.89	-	-
Pb ₉ ⁴⁻	C _{4v}	0.89	0.88	0.67

Next in line is the group of trigonal-bipyramidal clusters starting from Bi₅³⁺, whose ELF topology has certain differences as compared to all other isoelectronic clusters. ELF topology for Bi₅³⁺ shows two types of localization domains, trisynaptic $\Omega 1$ corresponding to the three-center bonding basin over the center of the triangular face (population 0.72 e), and disynaptic $\Omega 2$ (population 0.70 e) corresponding to pairwise Bi-Bi interactions along the face, which, however, quickly merges with bismuth lone pair. Thus, Bi₅³⁺ is held together by multi-center and pairwise bonding alike. However, no other isoelectronic cluster features $\Omega 2$ -type basins, and all of them are apparently held together by three-center bonds. These bonds are close to 3c,2e for Sb₅³⁺, but the population of the respective basins in E₅²⁻ (E = Ge, Sn, Pb) is lower and further decreases with increased atomic number (see Table 2). This might be associated with the anionic nature of these clusters.

Bi₅³⁺ was also studied by NBO and ELF in [42]. Once again, NBO correctly predicted the presence of three-center bonds but completely broke the symmetry. ELF correctly showed three-center bonds at lower η values, which were called delocalized on that basis. Now, having calculated basin populations, we can agree that, at least, a three-center bond involving 0.7 e can be in a certain sense regarded as less well-localized than the same kind of bond involving 1.7 e. In the same sense, we can observe the decrease in bond basin population from Ge to Pb and take it as a possible indication of decreasing bond localization. Nevertheless, there are proper electron localization domains for all these bonds.

3.3.2. Six-vertex Polyhedra

A single cluster of this type is known; Bi₆²⁺. ELF topological analysis (see Figure 5, Table 2) shows two kinds of bond basins, disynaptic $\Omega 1$ (1.45 e) corresponding to pairwise interactions in the equatorial plane, and disynaptic $\Omega 2$ (0.95 e), corresponding to the pairwise bonds between apical and equatorial atoms. This picture is very close to what was observed for Bi₅⁺. Once again, we have a cluster based on essentially localized two-center interactions. Only alternative geometries for Bi₆²⁺ were studied in [42], so there is no material for comparison.

3.3.3. Eight-vertex Polyhedra

One bismuth cluster of this type is known, Bi₈²⁺, and its isoelectronic antimony analogue, Sb₈²⁺. ELF topological analysis shows two kinds of bond basins, $\Omega 1$ (1.61 e) corresponding to pairwise bonds in the square bases (see Figure 5), and $\Omega 2$ (0.21 e) corresponding to pairwise interactions connecting

the bases. Unlike Bi_5^{3+} , these basins, although they appear in triangular faces, are not trisynaptic and do not correspond to three-center bonds, but rather disynaptic. Notably, Ω_2 -type basins have very small populations as compared to Ω_1 , which indicates that localized bonding between the bases of the prism is much weaker than in the bases. Yet, the fact that there are localized bonds connecting the bases of the prism explains the lack of rotational disorder in the Bi_8^{2+} polycation. These localized interplanar bonds were completely missed in the ELF topology in [42], most likely, due to the lack of basis augmentation. Sb_8^{2+} shows the same ELF features; two types of two-center bond basins, disynaptic Ω_1 (1.52 e) and Ω_2 (0.51 e). Notably, interplanar bonds, in this case, involve more electrons, although they are still short even of 2c,1e bond.

3.3.4. Nine-vertex Polyhedra

These include Bi_9^{5+} and its isoelectronic analogues E_9^{4-} (E = Ge, Sn, Pb). Extensive discussion on the subject of nine-vertex cluster symmetry (D_{3h} vs. C_{4v}) has already been made [11,42,64], therefore, we have investigated both trigonal tricapped prism and square antiprism for Bi_9^{5+} (as well as experimentally observed C_s in Bi_6Br_7) and square antiprisms for E_9^{4-} .

Bismuth clusters, in the shape of a trigonal tricapped prism (as seen in Figure 5), have two types of bonding basins, trisynaptic Ω_1 (1.36 e) over the centers of trigonal bases, corresponding to three-center bonds, and disynaptic Ω_2 (1.17 e), corresponding to the two-center bonds connecting the caps with the prism. A similar picture, with slightly less populated basins, and minimal differences in Ω_2 populations (see Table 2) due to the breaking of the idealized symmetry of Bi_9^{5+} , is observed in Bi_6Br_7 . Nine-atomic bismuth clusters of the C_{4v} symmetry show slightly different pattern (see Figure 5) where three-center bonds, making up the sides of the prism (Ω_1 , 1.36 e), have a smaller corresponding basin population than pairwise bonds connecting the atoms in the base (Ω_2 , 1.57 e), and the basins corresponding to pairwise bonds connecting the cap (Ω_3 , 1.02 e) appear to be even less populated. No bonds between the atoms within the top square are observed. Most interesting is the situation with E_9^{4-} polyanions, where the topology of ELF only reveals pairwise interactions (see Figure 5), and each pairwise bond connecting the squares of the prism has its own basin (Ω_2). The population of bond basins in the anions is fairly evenly distributed and slightly decreases from Ge to Pb, as it was observed for E_5^{2-} .

The description of the ELF for Bi_9^{5+} (D_{3h}), given in [42], also confirms three-center bonds in the bases of the prism, however, they also consider bonds to caps being multi-center, which our study does not confirm, as we observe disynaptic localization domains connecting caps to rectangular faces. Interestingly, a similar picture was observed for this cation using ELI-D topological analysis [10], yet, based on the fact that the Ω_2 -type domains merge together in a ring when the localization parameter is decreased, these bonds were interpreted as three-center. However, it is clear from the figure that, before merging, these are domains centered on pairwise interactions, even if they are slightly off the straight line connecting atoms; in our ELF topology, they also merge at $\eta \sim 0.44$ (see Figure 5), yet at higher η they are recognizable as single attractors with defined corresponding basins.

It is also interesting to note that trigonal faces do not automatically mean three-center bonding in these clusters. To better illustrate the point, which at times can be obscured in 3D ELF plots, we have plotted ELF for triangular faces for several species (see Figure 6). As seen from the figure, Bi_8^{2+} (as well as Bi_{10}^{4+} , vide infra) has two bases connected by two-center bonds, while nine-atomic bismuth clusters show three-center bonding for a similar fragment, and Sn_9^{4-} shows only pairwise interactions. Particularly interesting is that Bi_9^{5+} has both three-center and two-center bonds for triangular faces, the former between the squares, and the latter between the cap and the square.

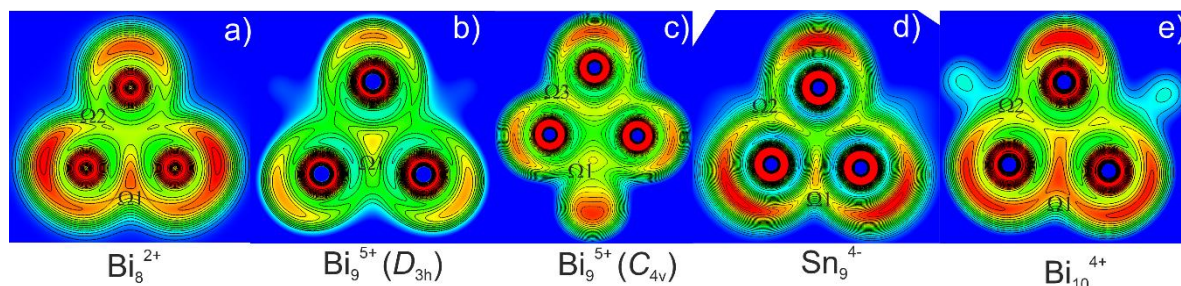


Figure 6. ELF cross-sections passing through atoms forming triangular faces of bismuth polycations: (a) triangular face connecting the bases in Bi_8^{2+} , (b) trigonal prism base in $\text{Bi}_9^{5+} (D_{3h})$, (c) triangular face connecting the cap to the square in $\text{Bi}_9^{5+} (C_{4v})$, (d) triangular face connecting the cap to the square in Sn_9^{4-} , (e) triangular face connecting the bases in Bi_{10}^{4+} . For the explanation of $\Omega 1$ – $\Omega 3$ see the text.

3.3.5. Ten-vertex Polyhedra

We have analyzed ELF for “empty” Bi_{10}^{4+} clusters, which have not been practically observed yet, as well as for characterized Pd- and Pt-centered ten-atomic bismuth polyhedra, which the authors of [28–31] call Pd@Bi_{10}^{4+} and Pt@Bi_{10}^{4+} . Our ELF analysis of Bi_{10}^{4+} (see Figure 5) shows the bonding picture very similar to the one observed for Bi_8^{2+} , i.e., almost perfect 2c,2e bonds in the bases ($\Omega 1$, 1.83 e), and two-center bonds connecting the bases ($\Omega 2$, 1.03 e). The latter are tricky to observe unobscured in 3D view, as they merge very quickly with $\Omega 1$, so we also provide 2D plot for a better view (see Figure 6). This cluster was investigated in [30] using ELI-D topological analysis, and the authors also observed bonding within five-member rings, however, they have reported no indications of bonding between them, concluding that there is no covalency between the rings. We can now revise that view, as such covalency is observed in our study.

Another very interesting question about these clusters is the nature of bonding between Pd or Pt and Bi. The authors of [28–30] did not see any indication of interactions between centering atom and bismuth. However, our investigation clearly shows localization domains between Bi and Pt at $\eta \sim 0.33$ ($\Omega 3$, see Figure 5). These are disynaptic basins with fairly low population of ca. 0.3 e, corresponding to, perhaps, not well-localized, yet still covalent bonds. The fact that they are observed at low η values is quite typical for Pt and Pd in metallic systems [65–68]. We could not observe the same kind of domains for PdBi_{10}^{4+} in a 3D view (see Figure 5), as we needed to decrease the localization parameter to the extent when the picture was completely cluttered with bismuth shells; however, there were basins similar to $\Omega 3$ found analytically, and they are also visible in the cross-section (see Figure 7). They have an even lower population than for Pt-Bi ones, 0.21 e, yet, in our view, this is still an indication of covalency and somewhat localized bonding. Moreover, the tendency for Pd to show less localized bonds than Pt in isotopic metallic systems was previously observed in ELI-D topology on several occasions [65,66]. Thus we can conclude that group 10 metals in both cases perform a more important function than mere fillers, and PdBi_{10}^{4+} and PtBi_{10}^{4+} , based on our direct-space bonding analysis, are most likely to be heteroatomic clusters.

To summarize this section, after providing the description of bonding in a series of main-group clusters, we would like to return to the question of 3D aromaticity and whether the description we provide, based on the picture of localized bonds revealed by ELF topologies, rules it out completely. We would not say so, as we only show that bonding patterns in such clusters are of more localized nature than was assumed before and can be rationalized using localized multi-centered and pairwise bonding interactions. Although previous conclusions regarding delocalization were made based on indirect indications, i.e., the lack of certainly observed bonding attractors, which we now can see, this does not preclude delocalization of a part of electrons. Indeed, relatively low basin populations for supposedly two-center interactions might serve as an indication of such delocalization (how such electrons would participate in bonding is another question). But since ELF only allows us to observe localized electron areas, this kind of indication would, once again, be indirect.

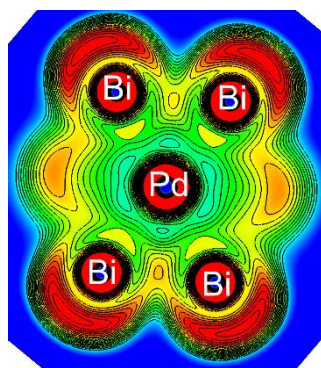


Figure 7. ELF cross-section passing through the Pd-Bi contacts in PdBi_{10}^{4+} .

4. Conclusions

To summarize this paper, an alternative synthetic approach allowed us to obtain good quality crystals of Bi_6Br_7 and to reinvestigate its crystal structure, and update the description of the structure as containing Bi_9^{5+} cluster polycations and polymer-like $^{1-}_{\infty}[\text{Bi}_3\text{Br}_{14}^{5-}]$ anions. Based on the DFT calculations, the compound was found to be semiconducting with a band gap of ca. 1.3 eV. The compound is best described as complex salt, with polymer-like anionic framework, most likely, responsible for electronic transport. Additionally, band structure and crystallographic analysis indicate a possibility of polycations, embedded in the anionic framework, also contributing to it. Direct-space bonding analysis using ELF for all known bismuth homoatomic polycations and their isoelectronic analogues has shown the pattern of two- and three-center localized bonding in these species, rather than a tendency for dominating 3D-aromaticity. We have also found indications of localized bonding between bismuth and group 10 metals in PdBi_{10}^{4+} and PtBi_{10}^{4+} , which characterizes these species as heteroatomic clusters rather than homoatomic bismuth species centered by non-interacting atoms.

Supplementary Materials: The following are available online at <http://www.mdpi.com/2073-4352/10/10/940/s1>, Table S1: Crystallographic parameters, X-ray data collection, and refinement details for a single-crystal experiment on Bi_6Br_7 , Table S2: Fractional atomic coordinates and anisotropic displacement parameters for Bi_6Br_7 . Tables S3–S14—side-by-side comparisons between the structures of Bi_6Br_7 from different sources and between the structure of Bi_6Cl_7 and Bi_6Br_7 .

Author Contributions: Conceptualization, A.N.K.; methodology, A.N.K. and E.A.S.; investigation, S.I.T., I.V.M., and A.N.K.; writing—original draft preparation, A.N.K.; writing—review and editing, S.I.T. and A.N.K.; visualization, A.N.K.; funding acquisition, I.V.M. All authors have read and agreed to the published version of the manuscript.

Funding: This research was funded by the Russian Science Foundation, grant number 19-43-04129.

Acknowledgments: The use of resources of Lomonosov Moscow State University HPC facilities for band structure calculations is acknowledged.

Conflicts of Interest: The authors declare no conflict of interest.

References

1. Corbett, J.D. Homopolyatomic ions of the post-transition elements—Synthesis, structure and bonding. In *Progress in Inorganic Chemistry*; Lippard, S.J., Ed.; Wiley & Sons: New York, NY, USA, 1976; Volume 21, pp. 129–159.
2. Hershaft, A.; Corbett, J.D. The Crystal Structure of Bismuth Subchloride. Identification of the Ion Bi_9^{5+} . *Inorg. Chem.* **1963**, *2*, 979–985. [[CrossRef](#)]
3. Friedman, R.M.; Corbett, J.D. Synthesis and structural characterization of bismuth(1+) nonabismuth(5+) hexachlorohafnate(IV), $\text{Bi}+\text{Bi}_9^{5+}(\text{HfCl}_6^{2-})_3$. *Inorg. Chem.* **1973**, *12*, 1134–1139. [[CrossRef](#)]
4. Von Benda, H.; Simon, A.; Bauhofer, W. Zur Kenntnis von BiBr und $\text{BiBr}_{1,167}$. *Z. Anorg. Allg. Chem.* **1978**, *438*, 53–67. [[CrossRef](#)]

5. Kuznetsov, A.N.; Shevelkov, A.V.; Troyanov, S.I.; Popovkin, B.A. New phases containing the Bi-9(5+) cluster polycation: Crystal structure of Bi₁₀Zr₃Br₁₈. *Russ. J. Inorg. Chem.* **1996**, *41*, 920–923.
6. Kuznetsov, A.N.; Shevelkov, A.V.; Popovkin, B.A. New Cluster Phases Containing Bi(9)(5+) Polycation: Disordered Structures. *Russ. J. Coord. Chem.* **1998**, *24*, 861–866.
7. Kuznetsov, A.N.; Naumenko, P.I.; Popovkin, B.A.; Kloo, L. New representative of Bi₉⁵⁺-containing phases: Synthesis and crystal structure of the Nb(IV)-containing Bi₁₀Nb₃Cl₁₈ compound. *Russ. Chem. Bull.* **2003**, *112*, 2100–2104. [[CrossRef](#)]
8. Ruck, M.; Dubensky, V. Bi₃₇InBr₄₈: Eine polares Subhalogenid mit Bi₉⁵⁺-Polykationen, komplexen Bromobismutat(III)-Anionen [Bi₃Br₁₃]⁴⁻ und [Bi₇Br₃₀]⁹⁻ sowie Pentabromoindat(III)-Anionen [InBr₅]²⁻. *Z. Anorg. Allg. Chem.* **2003**, *629*, 375–380. [[CrossRef](#)]
9. Hampel, S.; Schmidt, P.; Ruck, M. Synthese, thermochemische Eigenschaften und Kristallstruktur von Bi₇Cl₁₀. *Z. Anorg. Allg. Chem.* **2005**, *631*, 272–283. [[CrossRef](#)]
10. Wahl, B.; Ruck, M. Ag₃Bi₁₄Br₂₁: Ein Subbromid mit Bi₂⁴⁺-Hanteln und Bi₉⁵⁺-Polyedern—Synthese, Kristallstruktur und Chemische Bindung. *Z. Anorg. Allg. Chem.* **2008**, *634*, 2873–2879. [[CrossRef](#)]
11. Wahl, B.; Ruck, M. Finally Fulfilling Wade's Rules: The C_{4v} Symmetric Polycation Bi₉⁵⁺ in the Polar Structure of Bi₁₈Sn₇Br₂₄ = (Bi₉⁵⁺)₂[Sn₇Br₂₄¹⁰⁻]. *Z. Anorg. Allg. Chem.* **2010**, *636*, 337–342. [[CrossRef](#)]
12. Gerisch, A.; Ruck, M. (Bi₉)₄[Bi₃Pb₉Br₄₇]: Probing the limits of the concept “crystal”. *Z. Kristallogr.* **2011**, *226*, 613–618. [[CrossRef](#)]
13. Pabst, F.; Chang, J.-H.; Finzel, K.; Kohout, M.; Schmidt, P.; Ruck, M. The Subbromide Bi₅Br₄—On the Existence of a Hidden Phase. *Z. Anorg. Allg. Chem.* **2020**, *646*, 149–155. [[CrossRef](#)]
14. Corbett, J.D. Homopolyatomic ions of the heavy post-transition elements. Preparation, properties, and bonding of Bi₅(AlCl₄)₃ and Bi₄(AlCl₄). *Inorg. Chem.* **1968**, *7*, 198–208. [[CrossRef](#)]
15. Krebs, B.; Mummert, M.; Brendel, C. Characterization of the Bi₅³⁺ cluster cation: Preparation of single crystals, crystal and molecular structure of Bi₅(AlCl₄)₃. *J. Less Common Met.* **1986**, *116*, 159–168. [[CrossRef](#)]
16. Ulvenlund, S.; Ståhl, K.; Bengtsson-Kloo, L. Structural and Quantum Chemical Study of Bi₅³⁺ and Isoelectronic Main-Group Metal Clusters. The Crystal Structure of Pentabismuth(3+) Tetrachlorogallate(III) Refined from X-ray Powder Diffraction Data and Synthetic Attempts on Its Antimony Analogue. *Inorg. Chem.* **1996**, *35*, 223–230. [[CrossRef](#)] [[PubMed](#)]
17. Kuznetsov, A.N.; Popovkin, B.A.; Ståhl, K.; Lindsjö, M.; Kloo, L. Synthesis of Main-Group Polycations in Molten and Pseudo-Molten GaBr₃ Media. *Eur. J. Inorg. Chem.* **2005**, *2005*, 4907–4913. [[CrossRef](#)]
18. Lindsjö, M.; Fischer, A.; Kloo, L. Improvements of and Insights into the Isolation of Bismuth Polycations from Benzene Solution—Single-Crystal Structure Determinations of Bi₈[GaCl₄]₂ and Bi₅[GaCl₄]₃. *Eur. J. Inorg. Chem.* **2005**, *2005*, 670–675. [[CrossRef](#)]
19. Ruck, M.; Steden, F. Bi₅³⁺-Polykationen in geordneten und plastischen Kristallen von Bi₅[AlI₄]₃ und Bi₅[AlBr₄]₃. *Z. Anorg. Allg. Chem.* **2007**, *633*, 1556–1562. [[CrossRef](#)]
20. Friedman, R.M.; Corbett, J.D. On the synthesis and crystal structure of dodecabismuth tetradecachloride, Bi₁₂Cl₁₄. *Inorg. Chim. Acta* **1973**, *7*, 525–527. [[CrossRef](#)]
21. Krebs, B.; Hücke, M.; Brendel, C.J. Structure of the Octabismuth(2+) Cluster in Crystalline Bi₈(AlCl₄)₂. *Angew. Chem. Int. Ed. Engl.* **1982**, *21*, 445–446. [[CrossRef](#)]
22. Kuznetsov, A.N.; Popovkin, B.A. Bi₈(InBr₄)₂: A New Pseudo-hexagonal Bismuth Subbromide Containing Bi₈²⁺ Clusters. *Z. Anorg. Allg. Chem.* **2002**, *628*, 2179. [[CrossRef](#)]
23. Beck, J.; Hilbert, T. Crystal Structure and Magnetic Properties of Bi(Bi₉)[NbCl₆]₃, a New Member of the Structure Family Bi(Bi₉)[MX₆]₃, and the Crystal Structure of Bi₈[Ta₂O₂Br₇]₂. *Eur. J. Inorg. Chem.* **2004**, *2014*, 2019–2026. [[CrossRef](#)]
24. Knies, M.; Kaiser, M.; Anh, M.L.; Efimova, A.; Doert, T.; Ruck, M. Low-Temperature Ordering in the Cluster Compound (Bi₈)Tl[AlCl₄]₃. *Inorganics* **2019**, *7*, 45. [[CrossRef](#)]
25. Ruck, M. Bi₃₄Ir₃Br₃₇: Ein pseudosymmetrisches Subbromid aus Bi₅³⁺- und Bi₆²⁺-Polykationen sowie [IrBi₆Br₁₂]⁻—Und [IrBi₆Br₁₃]²⁻-Clusteranionen. *Z. Anorg. Allg. Chem.* **1998**, *624*, 521–528. [[CrossRef](#)]
26. Ruck, M.; Hampel, S. Stabilization of homonuclear Bi₅³⁺ and Bi₆²⁺ polycations by cluster anions in the crystal structures of Bi_{12-x}IrCl_{13-x}, Bi_{12-x}RhCl_{13-x} and Bi_{12-x}RhBr_{13-x}. *Polyhedron*. **2002**, *21*, 651–656. [[CrossRef](#)]
27. Hampel, S.; Ruck, M. Synthesen, Eigenschaften und Kristallstrukturen der Cluster-Salze Bi₆[PtBi₆Cl₁₂] und Bi_{2/3}[PtBi₆Cl₁₂]. *Z. Anorg. Allg. Chem.* **2006**, *632*, 1150–1156. [[CrossRef](#)]

28. Ruck, M.; Dubenskyy, V.; Söhnel, T. Structure and Bonding of Pd@[Bi₁₀]⁴⁺ in the Subbromide Bi₁₄PdBr₁₆. *Angew. Chem. Int. Ed.* **2003**, *42*, 2978–2982. [[CrossRef](#)] [[PubMed](#)]
29. Ruck, M.; Dubenskyy, V.; Söhnel, T. Das Subchlorid Bi₁₆PdCl₂₂: Pd@[Bi₁₀]⁴⁺-Polykationen in einem Raumnetzwerk aus Chlorobismutat(III)-Anionen. *Z. Anorg. Allg. Chem.* **2004**, *630*, 2458–2462. [[CrossRef](#)]
30. Wahl, B.; Erbe, M.; Gerisch, A.; Kloo, L.; Ruck, M. Nobel-Metal Centered Polycations [Au@[Bi₁₀]⁵⁺ or [Pd@[Bi₁₀]⁴⁺ Embedded in Halogenido-Bismuthate(III)-Stannate(II) Frameworks. *Z. Anorg. Allg. Chem.* **2009**, *635*, 743–752. [[CrossRef](#)]
31. Groh, M.F.; Wolff, A.; Wahl, B.; Rasche, B.; Gebauer, P.; Ruck, M. Pentagonal Bismuth Antiprisms with Endohedral Palladium or Platinum Atoms by Low-Temperature Syntheses. *Z. Anorg. Allg. Chem.* **2017**, *643*, 69–80. [[CrossRef](#)]
32. Ahmed, E.; Ruck, M. Homo- and heteroatomic polycations of groups 15 and 16. Recent advances in synthesis and isolation using room temperature ionic liquids. *Coord. Chem. Rev.* **2011**, *255*, 2892–2903. [[CrossRef](#)]
33. Groh, M.F.; Wolff, A.; Grasser, M.A.; Ruck, M. Controlled Synthesis of Polyions of Heavy Main-Group Elements in Ionic Liquids. *Int. J. Mol. Sci.* **2016**, *17*, 1452. [[CrossRef](#)] [[PubMed](#)]
34. Lindsjö, M.; Fischer, A.; Kloo, L. Sb₈(GaCl₄)₂: Isolation of a Homopolyatomic Antimony Cation. *Angew. Chemie Int. Ed. Engl.* **2004**, *43*, 2540–2543. [[CrossRef](#)] [[PubMed](#)]
35. Goicoechea, J.M. Homoatomic Polyaniions of the Early p-Block Elements. *Struct. Bond.* **2016**, *174*, 63–97. [[CrossRef](#)]
36. Beck, J.; Brendel, C.J.; Bengtsson-Kloo, L.; Krebs, B.; Mummert, M.; Stankowski, A.; Ulvenlund, S. The Crystal Structure of Bi₈(AlCl₄)₂ and the Crystal Structure, Conductivity, and Theoretical Band Structure of Bi₆Cl₇ and Related Subvalent Bismuth Halides. *Chem. Ber.* **1996**, *129*, 1219–1226. [[CrossRef](#)]
37. Groh, M.F.; Müller, U.; Ahmed, E.; Rothenberger, A.; Ruck, M. Substitution of Conventional High-temperature Syntheses of Inorganic Compounds by Near-room-temperature Syntheses in Ionic Liquids. *Z. Naturforsch.* **2013**, *68*, 1108–1122. [[CrossRef](#)]
38. Bader, R.F.W. *Atoms in Molecules: A Quantum Theory*; Oxford University Press: Oxford, UK, 1990.
39. Becke, A.D.; Edgecombe, K.E. A simple measure of electron localization in atomic and molecular systems. *J. Chem. Phys.* **1990**, *92*, 5397–5403. [[CrossRef](#)]
40. Kohout, M.; Savin, A. Atomic shell structure and electron numbers. *Int. J. Quantum Chem.* **1996**, *60*, 875–882. [[CrossRef](#)]
41. Savin, A.; Jepsen, O.; Flad, J.; Andersen, O.K.; Preuss, H.; von Schnering, H.G. Electron Localization in Solid-State Structures of the Elements: The Diamond Structure. *Angew. Chem. Int. Ed. Engl.* **1992**, *31*, 187–188. [[CrossRef](#)]
42. Kuznetsov, A.N.; Kloo, L.; Lindsjö, M.; Rosdahl, J.; Stoll, H. Ab Initio Calculations on Bismuth Cluster Polycations. *Chem. Eur. J.* **2001**, *7*, 2821–2828. [[CrossRef](#)]
43. Filatova, T.G.; Gurin, P.V.; Kloo, L.; Kulbachinskii, V.A.; Kuznetsov, A.N.; Kytin, V.G.; Lindsjö, M.; Popovkin, B.A. Electronic structure, galvanomagnetic and magnetic properties of the bismuth subhalides Bi₄I₄ and Bi₄Br₄. *J. Solid State Chem.* **2007**, *180*, 1103–1109. [[CrossRef](#)]
44. Sheldrick, G.M. *SHELX-2018/2. Program Package for Crystal Structure Solution and Refinement*; Georg-August-Universität Göttingen: Göttingen, Germany, 2018.
45. Kresse, G.; Joubert, D. From ultrasoft pseudopotentials to the projector augmented-wave method. *Phys. Rev. B* **1999**, *59*, 1758. [[CrossRef](#)]
46. Kresse, G.; Furthmüller, J. *Vienna Ab-Initio Simulation Package (VASP)*; v.5.4.4; Vienna University: Vienna, Austria, 2001.
47. Perdew, J.P.; Burke, K.; Ernzerhof, M. Generalized Gradient Approximation Made Simple. *Phys. Rev. Lett.* **1996**, *77*, 3865–3868. [[CrossRef](#)] [[PubMed](#)]
48. Monkhorst, H.J.; Pack, J.D. Special points for Brillouin-zone integration. *Phys. Rev. B* **1976**, *13*, 5188–5192. [[CrossRef](#)]
49. Becke, A.D. Density-functional thermochemistry. III. The role of exact exchange. *J. Chem. Phys.* **1993**, *98*, 5648–5652. [[CrossRef](#)]
50. Lee, C.T.; Yang, W.T.; Parr, R.G. Development of the Colle-Salvetti correlation-energy formula into a functional of the electron density. *Phys. Rev. B* **1988**, *37*, 785–789. [[CrossRef](#)]
51. Neese, F. The ORCA program system. *Wiley Interdiscip. Rev. Comput. Mol. Sci.* **2012**, *2*, 73–78. [[CrossRef](#)]

52. Neese, F. Software update: The ORCA program system, version 4.0. *Wiley Interdiscip. Rev. Comput. Mol. Sci.* **2017**, *8*, e1327. [[CrossRef](#)]
53. Rappoport, D.; Furche, F. Property-optimized Gaussian basis sets for molecular response calculations. *J. Chem. Phys.* **2010**, *133*, 134105. [[CrossRef](#)]
54. Metz, B.; Stoll, H.; Dolg, M. Small-core multiconfiguration-Dirac-Hartree-Fock-adjusted pseudopotentials for post-d main group elements: Application to PbH and PbO. *J. Chem. Phys.* **2000**, *113*, 2563–2569. [[CrossRef](#)]
55. Zheng, J.; Xu, X.; Truhlar, D.G. Minimally augmented Karlsruhe basis sets. *Theor. Chem. Acc.* **2011**, *128*, 295–305. [[CrossRef](#)]
56. Lu, T.; Chen, F. Multiwfn: A multifunctional wavefunction analyser. *J. Comput. Chem.* **2012**, *33*, 580–592. [[CrossRef](#)] [[PubMed](#)]
57. Momma, K.; Izumi, F. VESTA 3 for three-dimensional visualization of crystal, volumetric and morphology data. *J. Appl. Crystallogr.* **2011**, *44*, 1272–1276. [[CrossRef](#)]
58. wxDragon, ver.2.2.3. Available online: <http://www.wxdragon.de/> (accessed on 15 October 2020).
59. De la Flor, G.; Orobengoa, D.; Tasci, E.; Perez-Mato, J.M.; Aroyo, M.I. Comparison of structures applying the tools available at the Bilbao Crystallographic Server. *J. Appl. Cryst.* **2016**, *49*, 653–664. [[CrossRef](#)]
60. Lepetit, C.; Fau, P.; Fajewerg, K.; Kahn, M.L.; Silvi, B. Topological analysis of the metal-metal bond: A tutorial review. *Coord. Chem. Rev.* **2017**, *345*, 150–181. [[CrossRef](#)]
61. Hay, P.J.; Wadt, W.R. Ab initio effective core potentials for molecular calculations. Potentials for main group elements Na to Bi. *J. Chem. Phys.* **1985**, *82*, 284–298. [[CrossRef](#)]
62. Kuechle, W.; Dolg, M.; Stoll, H.; Preuss, H. Ab initio pseudopotentials for HG through RN. 1. Parameter sets and atomic calculations. *Mol. Phys.* **1991**, *74*, 1245–1263. [[CrossRef](#)]
63. Kohout, M.; Wagner, F.R.; Grin, Y. Electron localization function for transition-metal compounds. *Theor. Chim. Acc.* **2002**, *108*, 150–156. [[CrossRef](#)]
64. Rosdahl, J.; Fässler, T.F.; Kloo, L. On the Structure of Nonastannide Clusters in Liquid and Solid State. *Eur. J. Inorg. Chem.* **2005**, *2005*, 2888–2894. [[CrossRef](#)]
65. Zakharova, E.Y.; Andreeva, N.A.; Kazakov, S.M.; Kuznetsov, A.N. Ternary arsenides based on platinum-indium and palladium-indium fragments of the Cu₃Au-type: Crystal structures and chemical bonding. *J. Alloy. Compd.* **2015**, *621*, 307–313. [[CrossRef](#)]
66. Zakharova, E.Y.; Kazakov, S.M.; Götze, A.; Kohlmann, H.; Kuznetsov, A.N. Ternary palladium-indium-phosphorus and platinum-indium-phosphorus compounds based on the Cu₃Au-type: Structure, bonding, and properties. *J. Solid State Chem.* **2018**, *265*, 266–273. [[CrossRef](#)]
67. Zakharova, E.Y.; Kazakov, S.M.; Isaeva, A.A.; Abakumov, A.M.; Van Tendeloo, G.; Kuznetsov, A.N. Pd₅InSe and Pd₈In₂Se—New metal-rich homological selenides with 2D palladium-indium fragments: Synthesis, structure and bonding. *J. Alloys Compd.* **2014**, *589*, 48–55. [[CrossRef](#)]
68. Plokhikh, I.V.; Khan, N.; Tsirlin, A.A.; Kuznetsov, A.N.; Charkin, D.O.; Shevelkov, A.V.; Pfitzner, A. Synthesis, crystal and electronic structures of Pt-rich phosphides EuPt₃P and EuPt₆P₂. *Dalton Trans.* **2019**, *48*, 15272–15282. [[CrossRef](#)] [[PubMed](#)]

Publisher's Note: MDPI stays neutral with regard to jurisdictional claims in published maps and institutional affiliations.



© 2020 by the authors. Licensee MDPI, Basel, Switzerland. This article is an open access article distributed under the terms and conditions of the Creative Commons Attribution (CC BY) license (<http://creativecommons.org/licenses/by/4.0/>).